An unusually massive stellar black hole in the Galaxy

J. Greiner*, J. G. Cuby† & M. J. McCaughrean*

** Astrophysical Institute Potsdam, 14482 Potsdam, Germany*
† ESO, Alonso de Córdova 3107, Santiago 19, Chile

The X-ray source known as GRS1915+105 belongs to a group dubbed 'microquasars'[1,2]. These objects are binary systems which sporadically eject matter at speeds that appear superluminal, as is the case for some quasars. GRS1915+105 is also one of only two known binary sources thought to contain a maximally spinning black hole[3]. Determining the basic parameters of GRS195+105, such as the masses of the components, will help us to understand jet formation in this system, as well as providing links to other objects which exhibit jets. Using X-ray data, indirect methods[4,5] have previously been used to infer a variety of masses for the accreting compact object in the range 10–30 solar masses ($M_\odot$). Here we report a direct measurement of the orbital period and mass function of GRS1915+105, which allow us to deduce a mass of $14 \pm 4\,M_\odot$ for the black hole. Black holes with masses >5–$7\,M_\odot$ challenge the conventional picture of black-hole formation in binary systems[6–9]. Based on the mass estimate, we interpret the distinct X-ray variability of GRS1915+105 as arising from instabilities in an accretion disk that is dominated by radiation pressure, and radiating near the Eddington limit (the point where radiation pressure supports matter against gravity). Also, the mass estimate constrains most models which relate observable X-ray properties to the spin of black holes in microquasars.

GRS1915+105 is located in the Galactic plane at a distance of ~11–12 kpc (refs 10, 11) and suffers a large extinction of 25–30 mag in the visual band. Spectroscopic observations in the near-infrared H and K bands identified absorption features from the atmosphere of the companion (mass-donating star) in the GRS1915+105 binary[12]. The detection of ^{12}CO and ^{13}CO band heads plus a few metallic absorption lines suggested a K-M spectral type and luminosity class III (giant).

The presence of these band-head features led us to carry out follow-up medium-resolution spectroscopy in the 2.29–2.41 μm wavelength range using the Very Large Telescope (VLT)-Antu equipped with Infrared Spectrometer and Array Camera ISAAC, between April and August 2000 (Fig. 1). Radial velocities were measured for the 16 individual spectra by cross-correlation of the major CO band heads, and a period analysis was carried out (Fig. 2). The periodogram shows a clear peak at a period of 33.5 days (top panel) which we interpret as the orbital period $P_{\rm orb}$ of the binary system. The velocity amplitude is measured to be $K_{\rm d} = 140 \pm 15\,{\rm km\,s^{-1}}$ (lower panel). Figure 1 shows that the infrared flux is dominated by light from the accretion flow or jet, rather than from the secondary star. There is thus a possibility that phase-dependent changes in the continuum near the absorption features may result in an additional source of systematic error in the measured value of $K_{\rm d}$. The measured parameters allow us to determine the mass function $f(M)$, that is, the observational lower limit to the mass of the compact object:

$$f(M) \equiv \frac{(M_{\rm c}\sin i)^3}{(M_{\rm c}+M_{\rm d})^2} = \frac{P_{\rm orb}K_{\rm d}^3}{2\pi G} = 9.5 \pm 3.0\,M_\odot \qquad (1)$$

In order to determine the true mass of the black hole, $M_{\rm c}$, estimates of the donor mass $M_{\rm d}$ and the orbital inclination i are required. (G is the gravitational constant.) The K-M III classification at a first approximation implies a mass of $M_{\rm d} = 1.2 \pm 0.2\,M_\odot$ for the donor[12]. Because of the high mass-loss of the donor (needed to explain the large X-ray luminosity), the donor is almost certainly less luminous than a non-interacting star of the same spectral type. This in turn would imply a larger donor mass, thus making the black-hole mass estimate (see below) a lower limit when using $M_{\rm d} = 1.2\,M_\odot$. The orbital inclination of the GRS1915+105 binary can be deduced from the orientation of the jet, which in turn is derived from the brightness and the velocities of both the approaching and receding blobs[10,11]. This angle of 70° ± 2° was observed to be constant over several years, indicating no measurable precession,

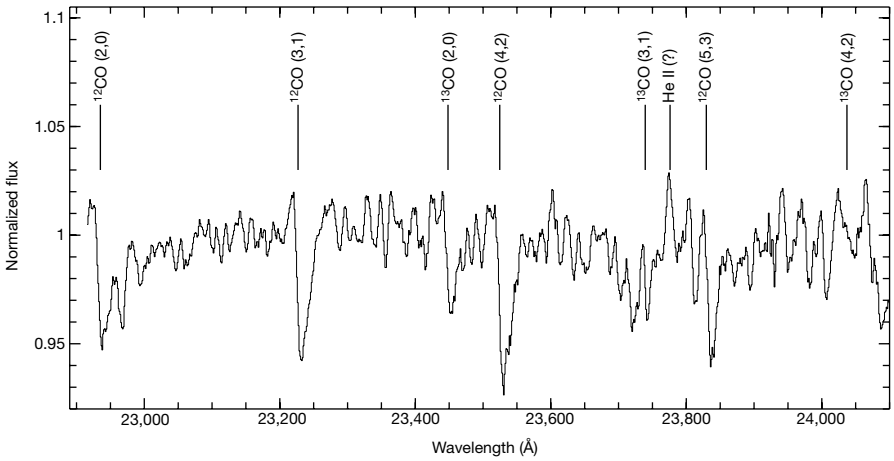

Figure 1 Mean K-band spectrum of GRS1915+105. It was obtained at the ESO VLT-Antu telescope, using the short-wavelength (0.9–2.5 μm) arm of ISAAC, equipped with a 1,024 × 1,024 pixel Rockwell HgCdTe array with an image scale of 0.147″ per pixel. The medium resolution grating (1.2 Å per pixel in the K band) was used, which yielded a spectral resolution of ~3,000 with a 1″ slit. Exposures of GRS1915+105 consisted of eight 250-s individual exposures which were dithered along the slit by ±10″. In order to correct for atmospheric absorption, the nearby star HD179913 (A0 V) was observed either before or after each exposure. The initial data reduction steps such as bias subtraction, flatfielding and co-adding were performed within the Eclipse package[26]. The extraction and wavelength calibration was done using an optimal extraction routine within the MIDAS package[29]. The spectrum shown here is the sum of 5 exposures with 167 min total integration time. Band heads of CO are marked with vertical lines and the numbers in brackets denote the energy levels of the transition. The presence of the ^{13}CO isotope and the equivalent width ratio of ^{12}CO to ^{13}CO suggests a classification of the donor as a late-type giant. The small width and faintness of the CO band heads imply that the donor contributes only a few per cent to the total K-band brightness (see ref. 12 for details) of the binary system GRS1915+105.

and justifies the assumption that the jet is perpendicular to the accretion disk and orbital plane. Knowing the inclination i and a lower limit of the donor mass, we can now solve equation (1) for the mass of the accreting compact object (Fig. 3), finding $M_c = 14 \pm 4\,M_\odot$. Table 1 summarizes all orbital parameters of GRS1915+105. Even after accounting for the relatively large error dominated by the determination of the velocity amplitude K_d, GRS1915+105 is the Galactic low-mass X-ray binary with the largest known mass function and the largest known mass of its compact object. Previous record holders were V404 Cyg with $f(M) = 6.07 \pm 0.05$, $M_c = 7$–$10\,M_\odot$ (ref. 13) and XTE J1118+480 with $f(M) = 6.00 \pm 0.36$, $M_c = 6.5$–$10\,M_\odot$ (ref. 14).

The mass of the black hole in GRS1915+105 has several implications for our understanding of the physics of microquasars, as well as some broader astrophysical concepts. Most importantly, the formation of a $14\,M_\odot$ black hole in a low-mass binary poses a challenge for binary evolution models. Stellar evolution of stars in a binary system proceeds differently from single star evolution primarily due to the mass transfer between the system components and/or common-envelope phases. There are, in general, two different paths for the black-hole formation in a binary system. First, the progenitor system could be wide, and during the common-envelope phase the low-mass (main sequence) star of $\sim M_\odot$ will spiral into the envelope of the massive giant (progenitor of the black hole), causing the orbit to shrink[9,15]. Based on our measured system parameters (Table 1), the deduced orbital separation of the binary components in GRS1915+105 is $108 \pm 4\,R_\odot$ ($R_\odot$ is the radius of the Sun, 6.9×10^5 km). Thus, orbital contraction through a common-envelope phase caused by the expansion of the massive progenitor to typically $\gtrsim$1,000 $R_\odot$, is conceivable for GRS1915+105. Second, the evolution could start with a progenitor system smaller than today, provided the binary component interaction is delayed until after helium burning has ceased[6]. In this case, the time between the

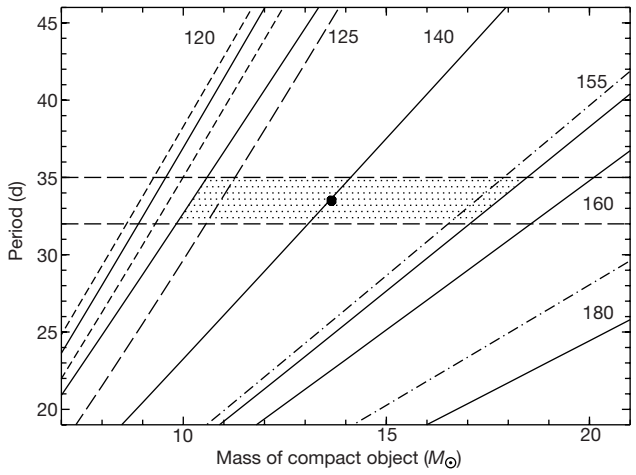

Figure 3 Black-hole mass constraints for GRS1915+105. The relation of orbital period versus mass of the black hole is plotted for various velocity amplitudes K_d (solid lines) in km s^{-1}. We assumed an orbital inclination of 70° and a mass of the donor of 1.2 $M_\odot$. The horizontal long-dashed lines indicate the boundaries of the period uncertainty, and the radial velocity range is 125–155 km s^{-1}. Thus, the dotted region shows the allowed parameter space, leading to a mass of the accreting compact object of $14 \pm 4\,M_\odot$. The implied Roche lobe size of the donor star is $21 \pm 4\,R_\odot$, in good agreement with the size of a K-M giant which is thus likely to fill its Roche lobe. The uncertainty in the mass of the donor is shown for $K_d = 120$ km s^{-1} where the slanted dashed lines correspond to 1.0, 1.4 and 2.5 $M_\odot$, respectively (from left to right). While the formal uncertainty in the orbital inclination is only 2°, we show the effect of relaxing the assumption that the jet is perpendicular to the orbital plane by showing for the $K_d = 160$ km s^{-1} case the corresponding curves using $i = 79°$ (at which angle eclipses would set in; left dash-dot curve) and $i = 61°$ (right dash-dot curve). When relaxing the assumptions and using the extremes, the mass range would be 8–24 $M_\odot$.

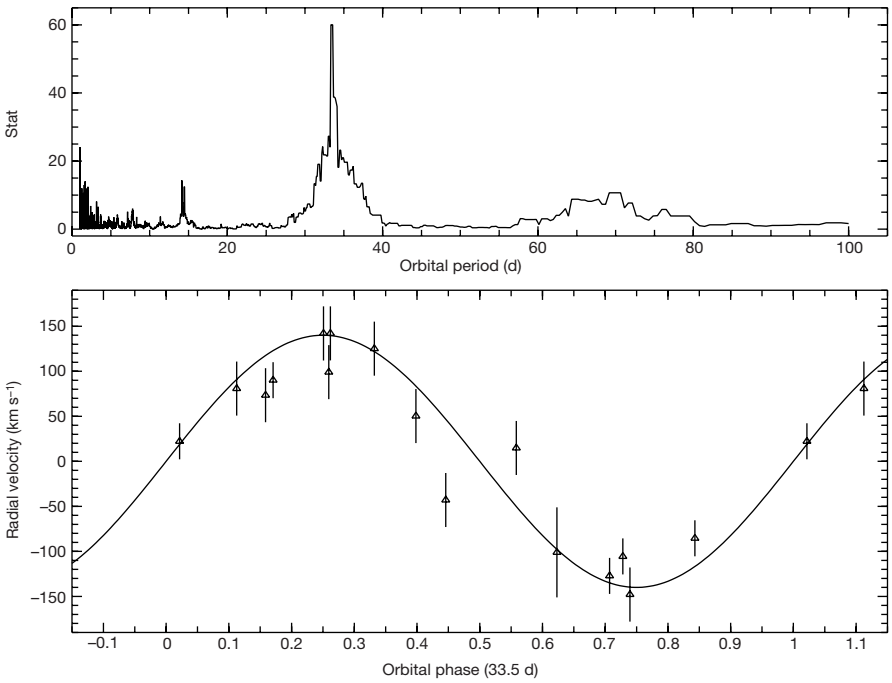

Figure 2 Period analysis of the velocity variation of the four CO band heads. Radial velocities were measured for the individual spectra by cross-correlation of the major CO band heads, using as template a spectrum of the K2III star HD202135 taken with the same setting. Top: Scargle periodogram after heliocentric correction of the individual measurements. Bottom: radial velocity curve folded over the best-fit period of $P_{orb} = 33.5$ days. The semi-amplitude of the velocity curve K_d is 140 ± 15 km s^{-1}. Distortions of the radial velocity curve due to X-ray heating (see, for example, ref. 27) are expected to be unimportant because of the long orbital period. The systemic velocity is $\gamma = -3 \pm 10$ km s^{-1} which implies that based on the Galactic rotation curve[28] the kinematic distance (d) of GRS1915+105 is $d = 12.1 \pm 0.8$ kpc, intermediate between earlier estimates[10,11]. 'Stat' is a measure of the significance of the period.

wind phase and the core-collapse is short, and black-hole masses in the 5–10 $M_\odot$ range are plausible when the initial helium-star progenitor is in the 10–25 $M_\odot$ range, corresponding to initial primaries with 25–45 $M_\odot$ (refs 8, 9). The total mass that is finally lost depends on the evolution of the two progenitor star radii, and it remains to be shown whether black-hole masses above 10 $M_\odot$ can be achieved. In order to produce even higher black-hole masses, the progenitor might have been a massive Wolf–Rayet star. However, Wolf–Rayet stars have a much larger wind-loss rate, and it is therefore unclear whether higher progenitor masses indeed will lead to higher final black-hole masses. An alternative way of producing high mass ($\gtrsim$10 $M_\odot$) black holes may be to invoke hierarchical triples as progenitors[16].

Knowledge of the mass of the accretor in GRS1915+105 also yields insight into the rapid and large-amplitude X-ray variability seen in this source[17], which occurs near or even above the Eddington accretion rate limit $\dot{M}_{\rm Edd}$. Such high accretion rates are not reached by other canonical black-hole transients (for example, GRO J1655–40) which usually operate in the 0.1–0.2 $\dot{M}_{\rm Edd}$ range, at which their accretion disks are probably gas pressure dominated, and thus viscously and thermally stable. The high $\dot{M}/\dot{M}_{\rm Edd}$ ratio in GRS1915+105 suggests that its inner accretion disk is radiation pressure dominated, which in turn makes the inner disk quasi-spherical and thermally unstable. This property provides a clue to the X-ray variability in GRS1915+105 (ref. 17). It is tempting to conclude that jet ejection occurs because the black hole can not accept this copious supply of matter. But jet ejection also occurs in other sources (for example, at 0.2 $\dot{M}_{\rm Edd}$ in GRO J1655–40), and thus near/super-Eddington accretion cannot be the determining factor for relativistic jets.

Finally, if the black-hole mass in GRS1915+105 is indeed no larger than 18 $M_\odot$ (Fig. 3), we can place constraints on the black-hole spin in GRS1915+105 and GRO J1655–40. Previously, information on the black-hole spin has been deduced from two completely different sources. First, accretion disks around a (prograde) spinning black hole extend farther down towards the black hole, and thus allow the temperature of the disk to be higher. Both GRS1915+105 and GRO J1655–40 exhibit a thermal component in their X-ray spectra which is unprecedentedly high when compared to all other black-hole transients (during outbursts). It has thus been argued that this is due to their black-hole spin (most black-hole transients have non-rotating black holes[3]). Second, several black-hole binaries, including GRS1915+105 and GRO J1655–40, show near-stable quasi-periodic oscillations (QPOs) in their X-ray emission. The frequency of oscillation, f, is 300 Hz in GRO J1655–40 (ref. 18) and 67 Hz in GRS1915+105 (ref. 5). Most of the models proposed[19–22] to explain these QPOs depend upon the spin of the accreting black hole. The black-hole mass of GRS1915+105 (M_c, in units of $M_\odot$) makes the deduction of the black-hole spin in ref. 3 inconsistent with any of these models. (1) If the QPO frequency is associated with the keplerian motion at the last stable orbit around a (non-rotating) black hole according to the simple relation $f = 2.2/M_c$, where f is in kHz, we find agreement with the optically determined mass for GRO J1655–40, but an error of a factor of 2 for GRS1915+105; that is, the QPO frequency does not scale linearly with the mass of the black hole. (2) If the QPO frequency is associated with the trapped g-mode (diskoseismic) oscillations near the inner edge of the accretion disk[19,20], the model would require a nearly maximally spinning black hole in GRO J1655–40, and a non-spinning black hole in GRS1915+105. (3) Similarly, if associated with the relativistic dragging of inertial frames around a spinning black hole[21] which would cause the accretion disk to precess, the implied specific angular momentum a (spin) of the black hole in GRS1915+105 would be $a \approx 0.8$, considerably lower than the $a \approx 0.95$ deduced for GRO J1655–40. The implications of both of these models are in conflict with the nearly identical accretion-disk temperatures for both sources which in turn requires a larger spin for GRS1915+105 (ref. 3). (4) If the QPO frequency is associated with oscillations related to a centrifugal barrier in the inner part of the accretion disk[22], the product of QPO frequency and black-hole mass is predicted to be proportional to the accretion rate, implying that the accretion rate in GRO J1655–40 should be a factor of ~10 larger than in GRS1915+105. This is certainly not the case.

Thus, none of these four models provides a satisfactory solution if we adopt the interpretation that the high accretion-disk temperatures are a measure of the black-hole spin[3]. But if this interpretation is dropped and the spin becomes a free parameter, then the first three models could be applicable. The deduction of accurate accretion-disk temperatures from the applied disk model has also been questioned on other grounds[23,24]. Additionally, there exist alternative, so-called slim disk models, which also reproduce high-temperature disks for non-rotating black holes[25]. □

Table 1 Spectroscopic orbital parameters of GRS1915+105

Parameter	Result
T_0 (UT)*	2000 May 02 00:00
T_0 (heliocentric)*	HJD 2451666.5 ± 1.5
γ (km s^{-1})	–3 ± 10
K_d (km s^{-1})	140 ± 15
$P_{\rm orb}$ (d)	33.5 ± 1.5
$f(M)$ ($M_\odot$)	9.5 ± 3.0
M_d ($M_\odot$)	1.2 ± 0.2
M_c ($M_\odot$)†	14 ± 4

*Time of blue-to-red crossing.
† Using an inclination angle $i = 70° \pm 2°$ (refs 10,11) (see Fig. 3 legend).

Received 14 June; accepted 12 October 2001.

1. Mirabel, I. F. & Rodriguez, L. F. Microquasars in our Galaxy. *Nature* **392,** 673–676 (1998).
2. Greiner, J. *Microquasars in Cosmic Explosions, Proc. 10th Annu. Astrophys. Conf.* (eds Holt, S. & Zhang, W. W.) 307–316 (AIP 522, American Institute of Physics, Melville, New York, 2000).
3. Zhang, N. S., Cui, W. & Chen, W. Black hole spin in X-ray binaries: Observational consequences. *Astrophys. J.* **482,** L155–L158 (1997).
4. Greiner, J., Morgan, E. H. & Remillard, R. A. RXTE Spectroscopy of GRS 1915+105. In Galactic Sources with Relativistic Jets (eds Ogley, R. N. & Bell Burnell, J.) *New Astr. Rev.* **42,** 597–600 (1998).
5. Morgan, E. H., Remillard, R. A. & Greiner, J. RXTE observations of QPOs in the black hole candidate GRS 1915+105. *Astrophys. J.* **482,** 993–1010 (1997).
6. Brown, G. E., Lee, C.-H. & Bethe, H. A. The formation of high-mass black holes in low-mass X-ray binaries. *New Astron.* **4,** 313–323 (1999).
7. Wellstein, S. & Langer, N. Implications of massive close binaries for black hole formation and supernovae. *Astron. Astrophys.* **350,** 148–162 (1999).
8. Brown, G. E., Lee, C.-H. & Tauris, T. M. Formation and evolution of black hole X-ray transient systems. *New Astron.* **6**(7), 457–470 (2001).
9. Kalogera, V. in *Evolution of Binary and Multiple Star Systems* (eds Podsiadlowski, P. *et al.*) (ASP Conf. Ser., Astronomical Society of the Pacific, San Francisco, in the press); also as preprint astro-ph/0012064 at ⟨http://xxx.lanl.gov⟩ (2001).
10. Mirabel, I. F. & Rodriguez, L. F. A superluminal source in the galaxy. *Nature* **371,** 46–48 (1994).
11. Fender, R. P. *et al.* MERLIN observations of relativistic ejections from GRS 1915+105. *Mon. Not. R. Astron. Soc.* **304,** 865–876 (1999).
12. Greiner, J., Cuby, J. G., McCaughrean, M. J., Castro-Tirado, A. J. & Mennickent, R. E. Identification of the donor in the X-ray binary GRS 1915+105. *Astron. Astrophys.* **373,** L37–L40 (2001).
13. Shahbaz, T., Bandyopadhyay, R., Charles, P. A. & Naylor, T. Infrared spectroscopy of V404 Cygni: limits on the accretion disc contamination. *Mon. Not. R. Astron. Soc.* **282,** 977–981 (1996).
14. McClintock, J. E. *et al.* A black hole of >6 $M_\odot$ in the X-ray nova XTE J1118+480. *Astrophys. J.* **551,** L147–L150 (2001).
15. Kalogera, V. Donor stars in black hole X-ray binaries. *Astrophys. J.* **521,** 723–734 (1999).
16. Eggleton, P. P. & Verbunt, F. Triple star evolution and the formation of short-period, low mass X-ray binaries. *Mon. Not. R. Astron. Soc.* **220,** 13p–18p (1986).
17. Greiner, J., Morgan, E. H. & Remillard, R. A. Rossi X-Ray Timing Explorer observations of GRS 1915+105. *Astrophys. J.* **473,** L107–L110 (1996).
18. Remillard, R. A., Morgan, E. H., McClintock, J. E., Bailyn, C. D. & Orosz, J. A. RXTE observations of 0.1–300 Hz quasi-periodic oscillations in the microquasar GRO J1655–40. *Astrophys. J.* **522,** 397–412 (1999).
19. Okazaki, A. T., Kato, S. & Fukue, J. Global trapped oscillations of relativistic accretion disks. *Publ. Astron. Soc. Jpn* **39,** 457–473 (1987).
20. Nowak, M. A., Wagoner, R. V., Begelman, M. C. & Lehr, D. E. The 67 Hz feature in the black hole candidate GRS 1915+105 as a possible "diskoseismic" mode. *Astrophys. J.* **477,** L91–L94 (1997).
21. Cui, W., Zhang, S. N. & Chen, W. Evidence for frame-dragging around spinning black holes in X-ray binaries. *Astrophys. J.* **492,** L53–L56 (1998).
22. Titarchuk, L., Lapidus, I. & Muslimov, A. Mechanisms for high-frequency quasi-periodic oscillations in neutron star and black hole binaries. *Astrophys. J.* **499,** 315–328 (1998).
23. Sobczak, G. J. McClintock, J. E., Remillard, R. E., Bailyn, C. D. & Orosz, J. A. RXTE spectral

observations of the 1996–1997 outburst of the microquasar GRO J1655–40. *Astrophys. J.* **520,** 776–787 (1999).
24. Merloni, A., Fabian, A. C. & Ross, R. R. On the interpretation of the multicolour disc model for black hole candidates. *Mon. Not. R. Astron. Soc.* **313,** 193–197 (2000).
25. Watarai, K., Fukue, J., Takeuchi, M. & Mineshige, S. Galactic black-hole candidates shining at the Eddington luminosity. *Publ. Astron. Soc. Jpn* **52,** 133–141 (2000).
26. Devillard, N. Eclipse users guide. ⟨http://www.eso.org/projects/aot/eclipse/eug/index.html⟩ (2000).
27. Phillips, S. N., Shahbaz, T. & Podsiadlowski, Ph. The outburst radial velocity curve of X-ray Nova Scorpii 1994 (=GRO J1655–40): a reduced mass for the black hole? *Mon. Not. R. Astron. Soc.* **304,** 839–844 (1999).
28. Fich, M., Blitz, L. & Stark, A. A. The rotation curve of the Milky Way to 2 $R_{\odot}$. *Astrophys. J.* **342,** 272–284 (1989).
29. Warmels, R. H. in *Astronomical Data Analysis Software and Systems I* 115–119 (PASP Conf. Ser. 25, Astronomical Society of the Pacific, San Francisco, 1991).

Acknowledgements

This work is based on observations collected at the European Southern Observatory, Chile.

Correspondence and requests for materials should be addressed to J.G. (e-mail: jgreiner@aip.de).

Atomic structure holography using thermal neutrons

B. Sur*, R. B. Rogge†, R. P. Hammond‡, V. N. P. Anghel* & J. Katsaras†

* *Atomic Energy of Canada Limited, Chalk River Laboratories, Chalk River, Ontario K0J 1J0, Canada*
† *National Research Council, Steacie Institute for Molecular Sciences, Chalk River, Ontario K0J 1J0, Canada*
‡ *Department of Physics and Astronomy, McMaster University, Hamilton, Ontario L8S 4M1, Canada*

The idea of atomic-resolution holography has its roots in the X-ray work of Bragg[1] and in Gabor's electron interference microscope[2]. Gabor's lensless microscope was not realized in his time, but over the past twelve years there has been a steady increase in the number of reports on atomic-resolution holography. All of this work involves the use of electrons[3–6] or hard X-rays[7–11] to produce the hologram. Neutrons are often unique among scattering probes in their interaction with materials: for example, the relative visibility of hydrogen and its isotopes is a great advantage in the study of polymers and biologically relevant materials. Recent work[12] proposed that atomic-resolution holography could be achieved with thermal neutrons. Here we use monochromatic thermal neutrons, adopting the inside-source concept of Szöke[13], to image planes of oxygen atoms located above and below a single hydrogen atom in the oxide mineral simpsonite[14].

The inside-source concept[15] uses the atoms making up the sample as independent sources of coherent illumination. In the case of X-ray holography and certain types of electron holography (such as auger holography), the radiation is generated by atomic de-excitation that propagates in the form of nearly spherical waves. This radiation can pass through the sample unperturbed (reference beam), or be scattered by the surrounding atoms (object beam). The interference between the reference and object beams produces the hologram. Similarly, incoherent scattering of thermal neutrons produces spherical waves. Hydrogen has a large incoherent neutron-scattering cross-section: $\sigma_i = 80$ barns. Unlike forms of electromagnetic radiation that interact primarily with electrons, neutrons interact directly with nuclei and are, to first order, equally capable of imaging light atoms and heavy atoms. Consequently, atomic-resolution holographic images can be obtained of materials comprised entirely of light atoms (for example, hydrocarbons). Both holography and conventional direct methods solve the phase problem in crystallography. Inside-source holography has the added advantage that only orientational order is required, that is, translational symmetry is not necessary. Holography is therefore also suitable for imaging non-crystalline materials such as nematic liquid crystals. Because of the large σ_i of hydrogen, thermal neutron holography should be particularly effective for the *ab initio* solution of organic macromolecule structures.

The sample used to demonstrate the feasibility of neutron holography was a single crystal of natural simpsonite, a rare oxide mineral of aluminium and tantalum with chemical formula $Al_4Ta_3O_{13}(OH)$. Simpsonite was first discovered in western Australia[14] in 1939 and was examined using X-ray diffraction[16] the same year. More recently[17] X-ray diffraction has been used to refine the crystal structure in the trigonal space group *P3* with unit cell parameters $a = 7.386(1)$ Å and $c = 4.516(1)$ Å. Simpsonite contains only one H atom in the unit cell, which is convenient for this demonstration experiment.

We obtained our data at the N5 instrument located at the National Research Universal (NRU) reactor, Chalk River Laboratories, Canada. The experimental set-up is depicted in an annotated photograph in Fig. 1. Neutrons of wavelength $\lambda = 1.3$ Å with an estimated wavelength resolution of $\Delta\lambda/\lambda \approx 1.5\%$ were obtained from a (113) reflection of a germanium monochromator. The sample-to-detector angular resolution was limited by distance collimation, as defined by a combination of an aperture in neutron-absorbing cadmium masks and the sample size, to approximately 2° vertically and 2° horizontally. The sample orientation (ϕ) and

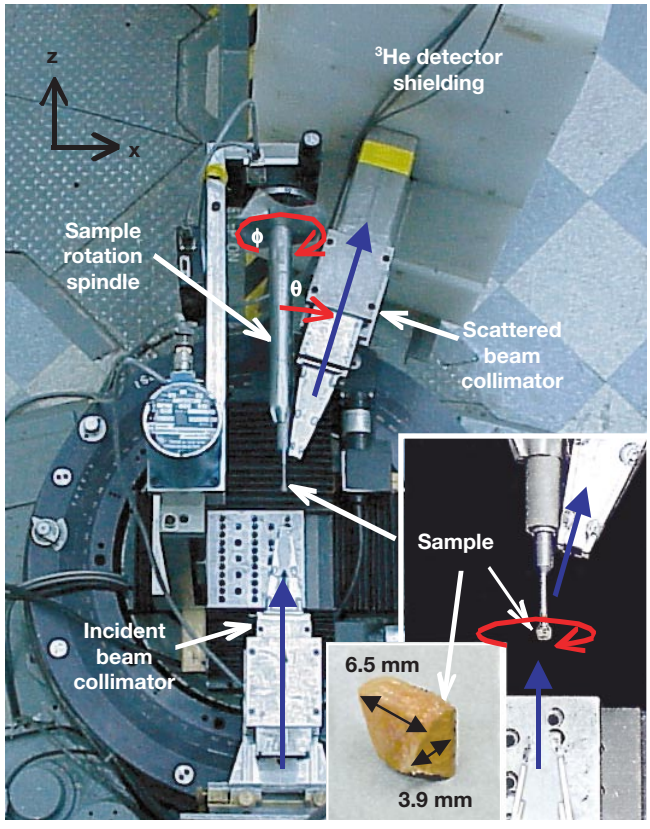

Figure 1 Plan view photograph of the experimental set-up. The incident neutron beam (originating from the bottom of the photograph) is parallel to the sample rotation axis (ϕ). The hologram data was obtained by rotating the sample through 2π radians, in optimal steps for the given detector coverage (2° × 2°), at a given detector angle θ. This was repeated, in 2° steps in θ, for $17° \leq \theta \leq 83°$. Interference between the scattered beam collimator and the sample rotation spindle imposed a lower limit on θ.